Geophysical Journal International

Geophys. J. Int. (2020) **220,** 450–460
Advance Access publication 2019 October 11
GJI Seismology

doi: 10.1093/gji/ggz460

Seismic anisotropy time variations at Mt Etna

Lucia Nardone,[1] Francesca Bianco,[1] Lucia Zaccarelli[2] and Domenico Patanè[3]

[1]*Istituto Nazionale di Geofisica e Vulcanologia, Osservatorio Vesuviano, Via Diocleziano* 328, I-80124 *Napoli, Italy. E-mail: lucia.nardone@ingv.it*
[2]*Istituto Nazionale di Geofisica e Vulcanologia, Sezione di Bologna, Via Franceschini* 31, I-40100 *Bologna, Italy*
[3]*Istituto Nazionale di Geofisica e Vulcanologia, Osservatorio Etneo, Piazza Roma* 2, I-95123 *Catania, Italy*

Accepted 2019 October 10. Received 2019 October 8; in original form 2019 January 16

SUMMARY

The aim of this paper is to study the temporal variations in the seismic wavefield associated with the stress changes in the dynamic features of the Mt Etna volcanic activity. We used shear wave splitting analysis on a huge data set of local earthquakes, in order to identify changes of the local stress field at Mt Etna during the time interval from 2006 to 2011. This analysis allows us to obtain two parameters: the polarization direction of the fast shear wave (φ) and the time delay of the slow shear wave (T_d, time delay between the split shear waves). Orientation of φ generally provides information about the anisotropic symmetry and stress direction whereas T_d provide information about the average crack density along the ray path.

Based on our findings it is possible to divide Etna Volcano in three different sectors, each one distinguished by typical fast wave polarization direction. We find that the western part of the volcano is controlled by the regional tectonic stress field having a NS and EW directions. Instead, the eastern part of the volcano is mainly controlled by the local volcanic stress, particularly an EW local stress field in the NE sector (Pernicana), and a quasi NS local stress field in the SE sector (Mascalucia, Timpe), where previous studies evidenced: (i) some low-Qp anomaly regions between 0 and about 6 km depth, probably associated with high pore pressure and the intense faulting and (ii) by magnetotelluric surveys, several high conductivity zones, up to 8 km depth, related to a diffuse presence of hydrothermal activity and fluid circulation. Temporal variations in time delay, mostly before the 2008–2009 lateral eruption, can be interpreted as stress accumulation increase with a consequent release of stress due to coalescing of microcracks in the conduit for the eruption of magma.

Key words: Seismic anisotropy; Volcano monitoring; Volcano seismology.

1 INTRODUCTION

Shear wave splitting (SWS), or birefringence phenomenon, occurs when a shear wave (*S* wave) enters in an anisotropic medium: the *S*-wave splits into 2 quasi shear waves (qS1 and qS2), with approximately orthogonal polarizations and different propagation velocity, never reconstructing the original waveform. The two observables associated with this phenomenon are: time delay (T_d) between the qS1 and qS2 arrivals, and the qS1 polarization direction (φ) in the horizontal plane.

SWS observations in the upper crust have been theoretically explained through the presence of fluid-filled vertically aligned microcracks (Crampin 1993). φ measurements allow to reconstruct the maximum compressive stress orientation direction of the investigated area. While T_d measurements, depending on the crack density and aspect ratios, give some rough indication on the magnitude of the local stress field. Using anisotropy poro-elasticity (APE) modelling for the evolution of stressed fluid-saturated cracks (Zatsepin & Crampin 1997) in the case of low pore—fluid pressure, the aligned cracks tend to be perpendicular to the direction of minimum compressional stress, and the fast shear wave is polarized parallel to the direction of maximum horizontal stress. When pore fluid pressure increases to critical levels, the effective stress-field realigns, microcrack distributions are modified and the fast shear wave does a 90°-flip and becomes parallel to direction of minimum horizontal stress (Crampin & Zatsepin 1997; Crampin & Peacock 2005). Some authors (do Nascimento *et al*. 2004) have claimed that even rock tectonic fabric may be an important source of seismic anisotropy.

Despite the fact that the theoretical approach (e.g. Crampin & Zatsepin 1997; Zatsepin & Crampin 1997) gives evidence that the splitting parameters may give information on the time variation of the local stress field, the role of shear wave splitting parameters as precursors of impending earthquakes or eruptions is still under debate. Experimental studies mainly show that splitting parameter's time variations associated with the occurrence of volcanic eruptions (e.g. Bianco & Castellano 1997; Gerst & Savage 2004; Bianco *et al*. 2006; Zaccarelli *et al*. 2009; Savage *et al*. 2010; Johnson *et al*. 2011; Liu *et al*. 2014; Rasmussen *et al*. 2018) are more coherent and

© The Author(s) 2019. Published by Oxford University Press on behalf of The Royal Astronomical Society.

Downloaded from https://academic.oup.com/gji/article-abstract/220/1/450/5585887 by INGV user on 03 December 2019

stable, compared to the earthquakes case (see for example Liu *et al*. 2014 and the comment by Crampin & Gao 2005). It is essential to know the background stress level in order to interpret a time modification as a possible anomaly, which may be further modelled as the response of the local stress field to rising magma from depth. The shear wave splitting analysis method, applied to volcanoes, has the potential to provide a new tool, which may enable to get information about the future appearance of an eruption (from a few months up to 1 yr) or the status of the volcano within an eruption cycle.

Our purpose is to study the variations of the stress field of Mt Etna Volcano by applying the SWS analysis to a data set of about 1600 local earthquakes that occurred in the 2006–2011 time period.

1.1 Mt Etna: structural features and previous anisotropy study

Mt Etna is one of the most active volcanoes in the world, the most active in Europe and it is characterized by an almost continuous eruptive activity from its craters, in the form of fairly frequent volcanic eruptions and open fissure eruptions on its flanks. Mt Etna is a composite volcano located in a region of complex geodynamics, where major regional structural features play an important role in the dynamic processes of the volcano (e.g. Gresta *et al*. 1998). Therefore, the characterization of the stress pattern on this volcano is a difficult task, because it depends on the interactions between the regional stress field and local stress due to magma movements into the upper crust and within the volcanic edifice, which cause different stress domains in time and space.

According to the regional tectonic framework, the stress and strain fields at Mt Etna appear to be homogeneous at depths greater than 10 km (Barberi *et al*. 2000; Patanè & Privitera 2001), with the main compressive stress and strain axes (σ_1 and ε_1) near the horizontal and *ca*. N–S orientated. This compressive stress field characterizes the central and western sectors of the volcano, whereas the eastern and southeastern sides of Etna seem to be linked to a tensional domain (Monaco *et al*. 1997) related to the Malta Escarpment structural system, transitional towards the Calabrian-Arc domain.

On the volcano surface different fault and fissure systems can be recognized (Fig. 1). The most outstanding tectonic features at Mt Etna are clearly recognizable on the east and southeast flanks of the volcano, where the clearest morphological evidence of active faulting exists (Fig. 1). Here, seismogenic faults can be related to the NNW–SSE Malta Escarpment (ME in Fig. 1) that is the main lithospheric structure in eastern Sicily. Other seismogenetic faults (Patanè *et al*. 2005), though not recognizable on the surface, can be linked to the NE–SW, ENE–WSW fault systems that control the tectonic evolution of the northern margin of the Hyblean Plateau (Torelli *et al*. 1998). The eastern flank of Mt Etna is characterized by frequent shallow seismic activity (depth <7–8 km) and by aseismic creep along some faults (Alparone *et al*. 2015). Conversely, the western flank of Mt Etna, normally characterized by a deeper seismicity (depth >5 km), is considered the most stable sector of the volcano. In the western sector, there is only slight morphological evidence of faulting, such as some short segments of faults observable on the south-western flank (e.g. Ragalna fault system). However, it must be noted that the faults with morphological evidence may represent only a part of the tectonic structures present in the Etnean area and hidden fault segments could be covered by the huge pile of volcanic products (e.g. Azzaro 1999).

Earthquakes at Mt Etna, usually volcano tectonic (VT) earthquakes, occur mainly in the form of swarms of small earthquakes that rarely exceed magnitude M_L 4 (e.g. Patanè *et al*. 2004). The genesis of this seismicity can be associated to: (i) regional tectonic stress; (ii) local stress, generated by the migration of the magma in the crust, or else triggered by dike propagation; (iii) stress due to slower inflating sources (Patanè *et al*. 2003, 2004; Gambino *et al*. 2004). The eastern part of the volcano is particularly active, and especially, the seismic activity in the southeast sector of the volcano, located between 3 and 8 km b.s.l., is associated with a E–W compression, induced by a pressurization source just westwards and at the same depth (Alparone *et al*. 2011, 2015).

In order to have a clear representation of the dynamic, of the volcanological model and of the time variation of the stress field at Etna volcano, many studies have been performed to improve the structural model of this volcanic system giving new indications of the interactions between its magma plumbing system and the regional tectonic regime.

Etna literature is rich in geophysical studies, such as gravimetric (Battaglia *et al*. 2008), geodetic (Viccaro *et al*. 2016), magnetic (Del Negro & Napoli 2004) and seismic measurements (Alparone *et al*. 2011; De Barros *et al*. 2011; O'Brien *et al*. 2011; Cannata *et al*. 2013; Patanè *et al*. 2013), including seismic attenuation studies (Del Pezzo *et al*. 1995, 1996, 2015; De Gori *et al*. 2005, 2011; Giampiccolo *et al*. 2007; Del Pezzo 2008), seismic tomographic imaging (Patanè *et al*. 2003, 2006; Ibáñez *et al*. 2016), as well as seismic anisotropy studies (Bianco & Castellano 1997; Bianco *et al*. 2006; Zaccarelli *et al*. 2009).

Bianco & Castellano in 1997 identified in the eastern part of Mt Etna Volcano a clear evidence of shear wave splitting, probably due to the presence of an anisotropic volume not homogeneously distributed. They suggested that the seismic anisotropy might be concentrated within 20 km depth.

In 2006, using about 2600 earthquakes occurred before the 2001 flank eruption, Bianco et al. showed:

-a systematic increase of the normalized time delay starting several days before the 2001 flank eruption on Mt Etna;
-variation of the polarization directions (90°-flips) of the fast shear wave at the station MNT, which was the closest to the eruption.

In 2014 Bianco *et al*., at the First Annual Meeting of MEDSUV Project, applied the shear wave analysis to a selected seismic data set, and defined the anisotropic background for data available from 1988 to 2004 (Fig. 2).

The data analysed by the authors constrain a leading polarization direction, and hence, the main direction of the anisotropic volume, approximately NS (see the inset in Fig. 2) oriented roughly for all sectors of Mt Etna, except for the Pernicana fault area, where the main direction is fault oriented and for the western sector, where only a few available data passed the selection (Zaccarelli & Bianco 2008), furnishing results that are not statistically significant. The depth extent of this volume seems to affect, on average, the first 8 km of the upper crust with a percentage of anisotropy ranging from 1.5 to 3 per cent (Bianco *et al*. 2006, 2014).

2 DATA SET AND DATA ANALYSIS

Our starting data set consisted of 1576 earthquakes recorded from 2006 to 2011 at the permanent seismic network of the INGV–Osservatorio Etneo. The network consisted of 38 three components stations (Fig. 3), but we discuss in this paper the results coming

Downloaded from https://academic.oup.com/gji/article-abstract/220/1/450/5585887 by INGV user on 03 December 2019

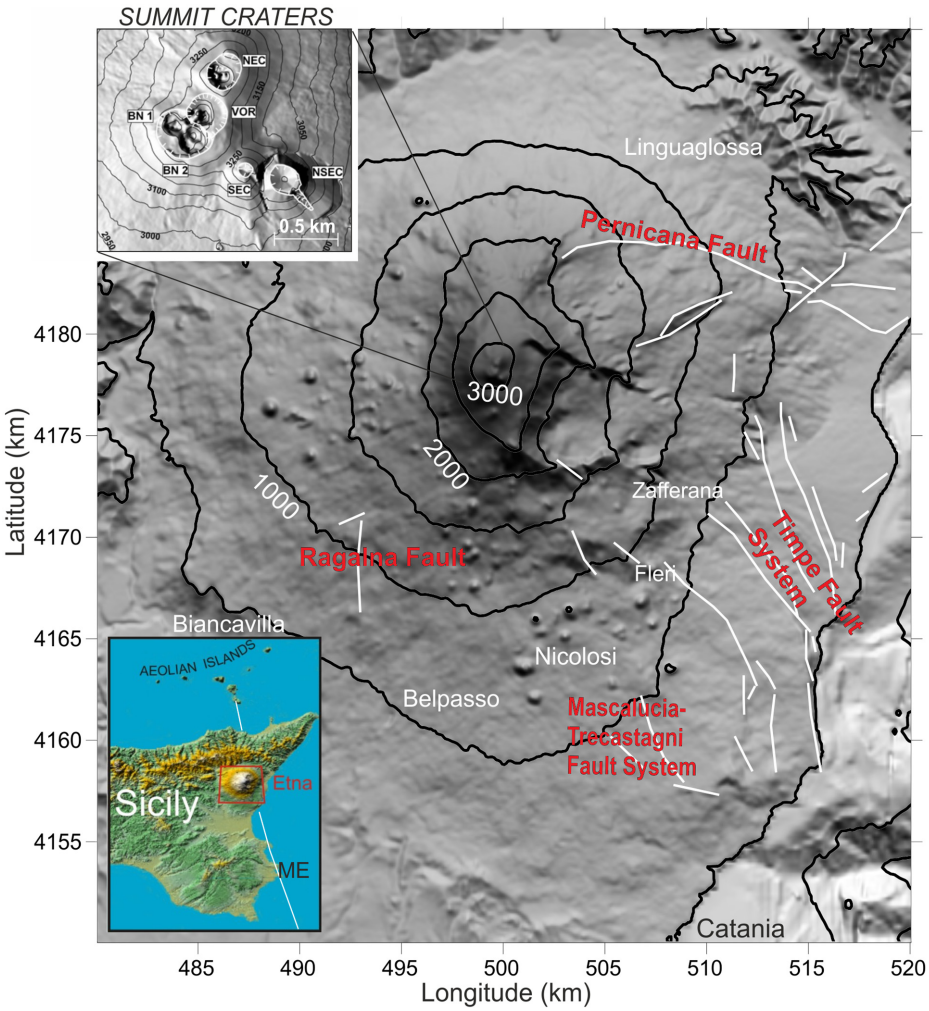

Figure 1. Map of Mt Etna with the location of the main faults (white line). The location of the summit craters is shown in the inset in the upper left-hand corner [VOR = Voragine, BN (1,2) = Bocca Nuova, SEC = Southeast Crater, NEC = Northeast Crater, NSEC = New Southeast Crater]. ME in the lower left inset is the Malta Escarpnet structure.

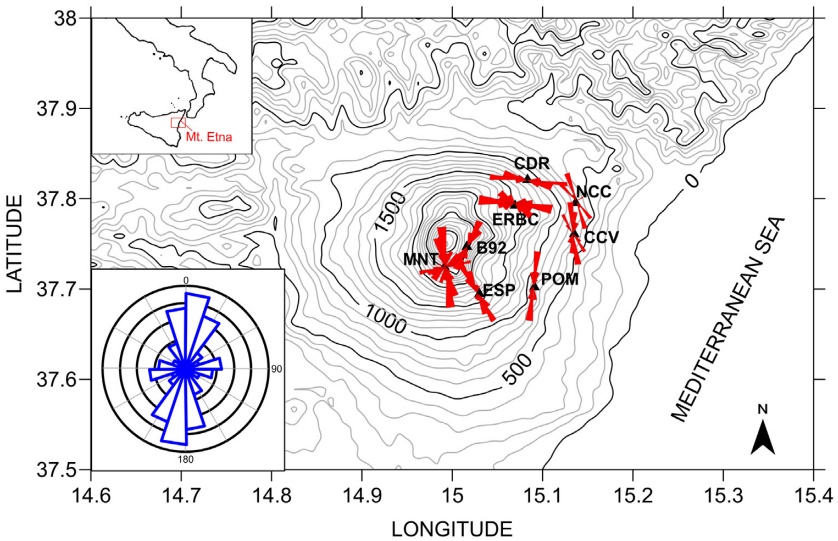

Figure 2. Anisotropy directions (φ) for different stations. Here only a selection of the obtained results are plotted, to avoid an extremely busy plot. In the lower left box is the resulting Background Anisotropy direction of all the measurements from all stations.

Downloaded from https://academic.oup.com/gji/article-abstract/220/1/450/5585887 by INGV user on 03 December 2019

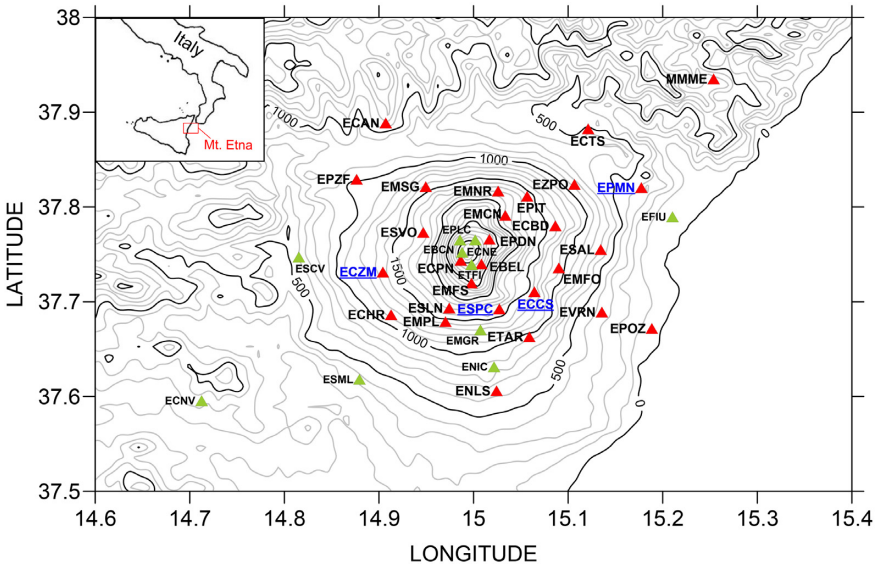

Figure 3. Map of Mt Etna's permanent seismic network. Only the seismic stations depicted with red triangles are used for the anisotropy analysis. The stations marched in blue are selected to show the temporal variations of the splitting parameters.

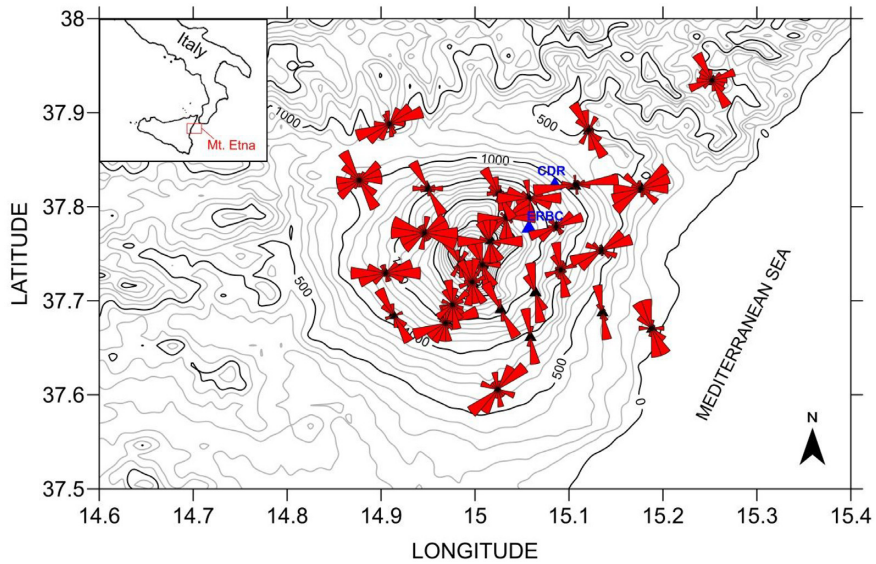

Figure 4. Rose diagrams of the azimuthal polarizations of the fast split shear wave (ϕ) obtained from the shallow and deep earthquakes. Each bin amplitude for the histograms is 20° wide. The stations in blue are two of the eight stations shown in the Fig. 2.

from only 28 stations (red triangles in Fig. 3) that provided more than 10 values of splitting parameters (see the data set in the "Splitting_parameter.xlsx" of the Supplementary data).

The earthquake data set has hypocentral distribution with depths varying from a minimum of about 1.6 km to a maximum of about 37 km below the sea level, and local magnitude varying from 0.5 to 4.8.

Even though the earthquakes are not necessarily caused by the volcanic system, but more likely by tectonic structures, their waves travelled through the volcanic structure, thus bringing with them information about the characteristics of the medium. Based on the results obtained by Bianco *et al*. (2006, 2014), and looking at the hypocentral distribution, we made a selection on the data on the basis of the fact that earthquake locations show clustering of the events within the first 10 km. Therefore the earthquakes were divided into 2 subdata sets as function of depth: the shallow earthquakes, named sub1, with hypocentral depth shallower than 10 km; and the deep earthquakes, sub2, with hypocentral depth deeper than 10 km (see Fig. S1 in the Additional_Supporting_Information of the Supplementary data). Furthermore, the spatial distribution of seismicity evidences that the eastern sector of the volcano is seismically very active, as most of the seismicity, both shallow and deep, is concentrated therein.

Due to the large number of earthquakes and stations in the data set, we applied a semi-automatic algorithm, SPY, to obtain the splitting parameters. SPY (Zaccarelli *et al*. 2012), is a Matlab code that evaluates the splitting parameters in a semi-automatic way. The algorithm requires as input the selected event waveforms, their hypocentre locations and *P* and *S* arrival times. Then it computes the polarization of the qS1-wave, by diagonalizing the covariance matrix of the horizontal components of the seismic signal in the chosen time window around the *S* waves, as the first eigen-vector.

Downloaded from https://academic.oup.com/gji/article-abstract/220/1/450/5585887 by INGV user on 03 December 2019

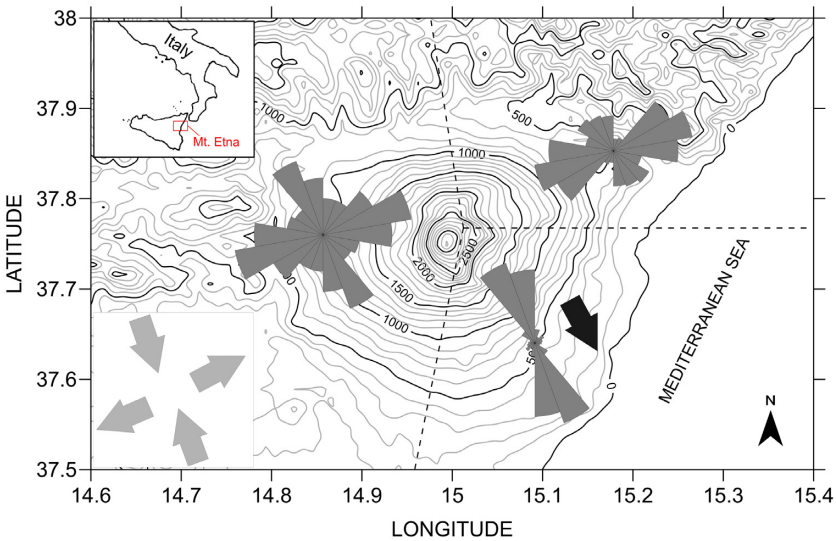

Figure 5. Resulting anisotropy polarizations of the three sectors, divided based on the main structural features of the volcano. Each bin amplitude for the histograms is 20° wide. The grey arrows in the lower left box indicate the direction of the regional stress field (Patanè & Privitera 2001; De Guidi *et al*. 2015; Scarfi *et al*. 2016). The black arrow indicate the prevalent direction of movement of the unstable flank of the volcano (Bonforte *et al*. 2011).

Rotating the traces into the fast direction, the time delay T_d between fast and slow arrivals is estimated through cross-correlation, and finally, by dividing T_d for the distances between the seismic station and the earthquake location, is estimated the normalized time delay T_n.

SPY has some internal selection rules that allow rejecting all the waveforms that do not exhibit clear *S* phases on the basis of three criteria (horizontal component amplitude greater than the vertical one, *S*-wave amplitude well above the *P*-coda values, and high rectilinearity of the fast wave polarization). Since the stations were displayed over an articulated topography and because of the low-velocity near-surface layers, we extended to a maximum 45° incidence angle the shear wave window (Crampin & Gao 2013). We performed this procedure for both shallow and deep subsets.

3 RESULTS

3.1 Fast shear wave polarization (φ)

As a result of the absence of significant differences in the polarization directions obtained from surface and deep earthquakes we have chosen to display for each station a single rose diagram of all the results. Therefore we superimposed the total obtained azimuthal polarization directions to the Mt Etna Volcano map only for stations with at least 10 results of splitting parameters (Fig. 4) and we plotted T_d evolution with time (Fig. 6) for the four most representative stations (labeled in blue in Fig. 3).

Due to their location with respect to the earthquake clusters, stations placed on the top and on the SE flank of the volcano (i.e. EBEL, ECCS, ECPN, EMFO, EMFS, ENLS, EPDN and EVRN) exhibit results mainly coming from shallow earthquakes. The stations EMNR, ESLN and ESPC show the same proportional number of SWS measurements from shallow and deep earthquakes, and finally the other stations show results mainly coming from deep earthquakes. Taking into account the Mt Etna main structural features (Fig. 1), and looking to the polarization directions obtained for each station (Fig. 4), the definition of a main azimuth as average value of φ over the whole volcanic edifice may not be appropriate. These observations allowed us to identify three homogenous sectors, thus, by averaging the station values in each sector, we define their representative polarization direction (Fig. 5).

In the SE sector the polarization direction is strongly oriented NNW–SSE, while the NE sector shows a polarization direction mainly ENE–WSW. The western sector instead presents two principal polarization direction perpendicular to each other.

The quasi EW direction, in the NE sector, may be easily related to the presence of the *ca*. EW Pernicana Fault or the NE Rift (Fig. 1). Several authors (Gledhill 1991; Zhang & Schwartz 1994; Zinke & Zoback 2000; Gao *et al*. 2011) showed that the predominant orientation of the fast polarization directions on active strike-slip faults, as the Pernicana fault, are parallel to the strike of the fault. In the unstable southeastern flank of the volcano (Rust *et al*. 2005; Neri *et al*. 2007; Nicolosi *et al*. 2014) the polarization directions show a predominant NNW–SSE direction, in agreement with both the main direction of the Timpe Fault System and the direction of the unstable block (black arrow in Fig. 5). Azzaro *et al*. (2013) have analysed geological and geophysical data to constrain the geometry and the kinematics of the fault systems controlling the East part of Mt Etna. They have deduced that the whole unstable flank of the volcano is characterized by a constant movement towards the sea, interrupted by sudden short-term accelerations related to flank eruptions, and have defined that the NE block (bordered by the Pernicana Fault) has a clockwise rotation along the EW direction and a general vertical (westward tilt) rotation of the SE sector.

The prevalent polarization directions identified by the SWS analysis, are consistent with the kinematic identified by Azzaro *et al*. (2013), because they are parallel to the fault strike and to the maximum horizontal compressive stress direction (local volcanic stress) responsible of the instability.

The two principal polarization directions of the western sector reflect the about N-S striking compressive regime obtained by Scarfi

Downloaded from https://academic.oup.com/gji/article-abstract/220/1/450/5585887 by INGV user on 03 December 2019

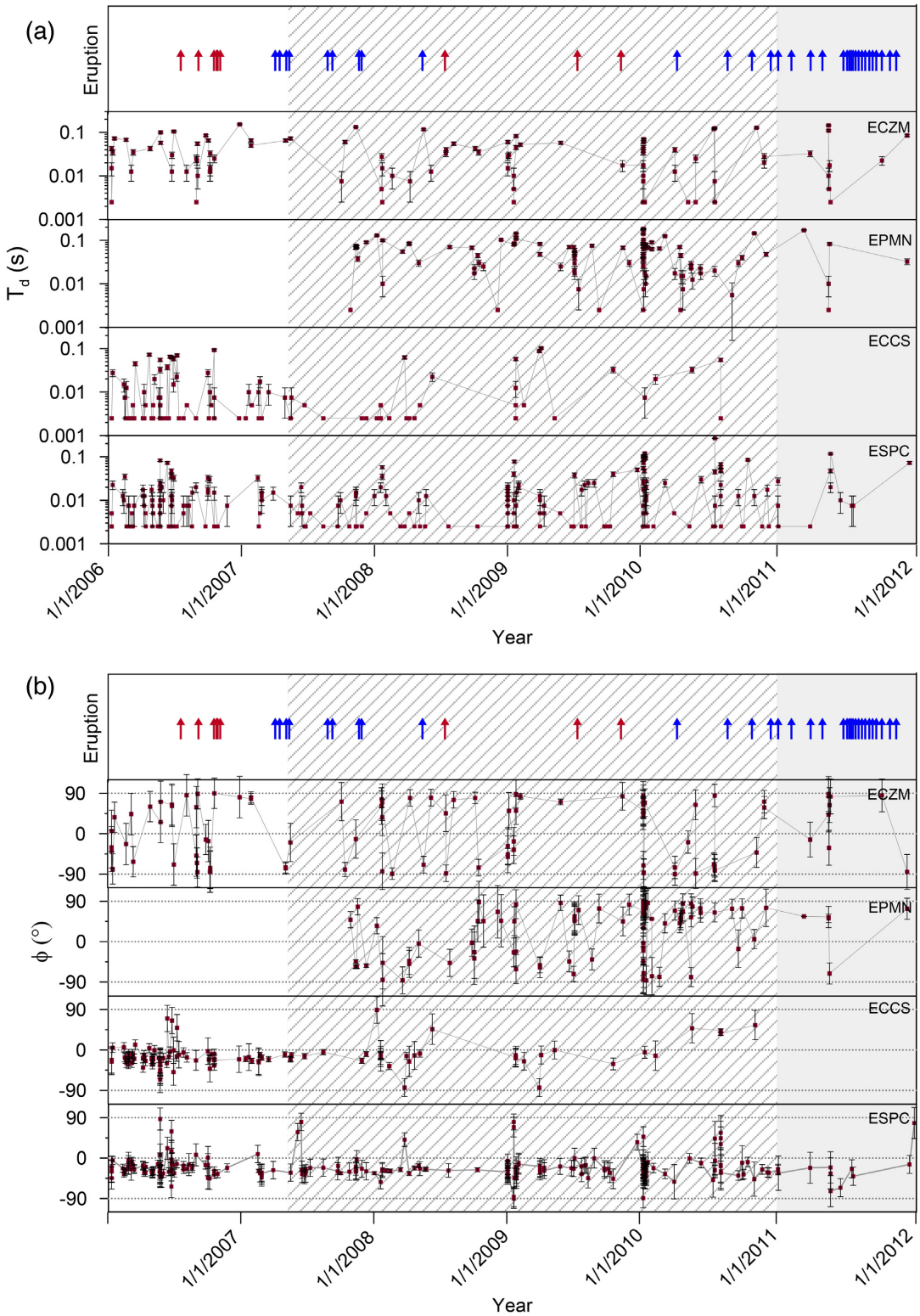

Figure 6. (a) Time delay and (b) polarizations of the fast split shear wave of a selected seismic data set. Electrical blue arrows: summit eruptions; Red arrows: lateral eruptions. White band: first phase including five lateral and three summit eruptions; Grey forward slash band: second phase including the formation of New South East Crater (NSEC) and the 2008–2009 lateral eruption; Grey band: third phase that brought to the enhancement of the NSEC with only summit eruptions.

Downloaded from https://academic.oup.com/gji/article-abstract/220/1/450/5585887 by INGV user on 03 December 2019

et al. (2016), using geological, seismological and geodetic data, due to the convergence between the African and Eurasian Plate, and the extensional regime due to the dynamics of the Malta Escarpment in the WNW–ESE direction (Díaz-Moreno *et al*. 2018; Neri *et al*. 2018).

Comparing the background polarization directions represented in Fig. 2 with the new results obtained for the 2006–2011 period, we note that for ESPC station, as well as for the SE sector stations, there are not variations in the polarization direction, while on the contrary stations placed in the NE sector show variations in the φ parameter values, which have changed from a EW (ERBC and CDR in Figs 2 and 4) to a ENE–WSW direction (Fig. 5). Finally, for the W Sector, the station MNT, the only one of the previous study lying in this sector, is in agreement with the prevalent two orthogonal directions, characterizing this part of the volcano.

3.2 Seismic anisotropy temporal variations

We analysed the temporal variations of the SWS parameters for the four most representative stations because they have the most measurements (ESPC, ECCS, ECZM and EPMN), trying to relate them to the volcanic activity at Etna (Fig. 6).

We have checked the increase of the delay time with distance for the selected stations using about 560 measures of T_d with respect to the hypocentral distance of earthquakes. We also calculated the correlation coefficients (CC) of T_d with the hypocentral distance (see Fig. S2 in the Additional_Supporting_Information of the Supplementary data). Most stations have a CC less than 0.3, indicating a lack of clear dependence on increasing distance. For this reason we have decided to not normalize the time delay for the distances and to keep the results in terms of T_d.

During the 2006–2007 time interval were reported only five lateral and three summit eruptions at the South East Crater (white background part of Fig. 6). In May 2007, the volcano started a new phase characterized by the definitive demise of the South East Crater and the shift to a new vent (New Southeast Crater, NSEC in Fig. 1), expected to occur after significant structural variations in the volcano dynamics (Acocella *et al*. 2016). Moreover, this phase was characterized by a long lateral eruption, which began in July 2008 and ended in July 2009 (grey part with the super-imposed diagonal lines in Fig. 6).

Finally, in the beginning of 2011 a further phase brought to the enhancement of the New Southeast Crater (grey part in Fig. 6; Patanè *et al*. 2013). A recent study, using LiDAR data (Behncke *et al*. 2016), has shown that in about 3 yr (from 2007 to 2010), the summit area of the volcano has accumulated over 86 million cubic metres of volcanic products, most of which (about 74 million) erupted by the eruptive fissure opened since 2008 to 2009 on the high western flank of the Valle del Bove, which was profoundly modified. For the selected four stations we performed a statistical analysis looking for change points in the variations of the T_d but the results are not stable due to the highly scattered values and only few are in common between the stations. Therefore, we do not observe a common behaviour of the stress field variations in the volcanic edifice related to the different eruptions, and this is in agreement with the open conduit state of this volcanic system. The few and clearly visible variations in the temporal trend of the SWS parameters pertain to single stations taken separately and thus they have to be related to extremely local changes of the stress field maybe due to the impending eruption taking place close by.

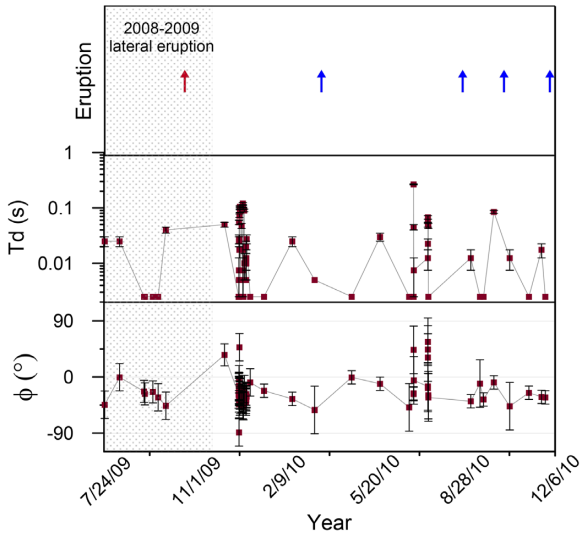

Figure 7. Time delay, T_d, and polarizations of the fast split shear wave ϕ at station ESPC in the 2009–2010 time interval. The grey points band identify the temporal interval of the lateral eruption.

In the first eruptive phase of the volcano, the station ECCS showed significant variations of T_d and some 90å-flips of φ up to about 30 d before the 2006 eruptions (started on 15 July 2006), decreasing to the average level after the eruption. Particularly the three changes are from $-29^\circ \pm 10^\circ$ to $70^\circ \pm 29^\circ$ occurred on 7 June 2006, from $-15^\circ \pm 10^\circ$ to $65^\circ \pm 29^\circ$ occurred on 21 June 2006 and from $-49^\circ \pm 29^\circ$ to $40^\circ \pm 29^\circ$ occurred on 4 July 2006. During the second phase eruption, which was characterized also by the 2008/2009 lateral eruption, ESPC, ECZM and EPMN stations showed marked variations. Particularly ESPC (Fig. 7) showed the highest value of almost 0.265 s and the strongest variations in T_d values after the lateral eruption end and towards the end of this second phase. We also observed that in correspondence of the maximum positive variation of T_d, ϕ values present a 90°-flip (bottom panel of Fig. 7).

Similar trends were observed in other regions before earthquakes (Crampin & Gao 2012), and before volcanic eruptions (Bianco *et al*. 2006; Zaccarelli *et al*. 2009; Liu *et al*. 2014). In the case of eruptions, the decrease of T_d as well as the 90°-flip can be interpreted as the release of stress due to a microcracks coalescing in the conduit for the eruption of magma.

3.3 Multiplet analysis

We analysed in more details the results coming from stations ESPC and ECZM. The first one is the most representative station, showing the higher number of results, while ECZM results exhibit the maximum variations in the T_d values. To identify the multiplets we performed a search in the database filtering the signals in the range of frequency 2–11 Hz and calculated the cross correlation function between all possible earthquakes using a 5-s-long time window starting 0.5 s before and ending 4.5 s after the *P*-wave arrival, applying a minimum similarity of 0.75 as a threshold value.

We found 35 earthquake multiplets for the station ESPC and 12 earthquake multiplets for the station ECZM, most of which are doublets. Finally, we selected only the multiplets with significant [outside the standard deviations (Zaccarelli & Bianco 2008)] variation in T_d or in φ: we named them d1–d7 and d8–d9 for station ESPC and ECZM, respectively, see Fig. 8.

Downloaded from https://academic.oup.com/gji/article-abstract/220/1/450/5585887 by INGV user on 03 December 2019

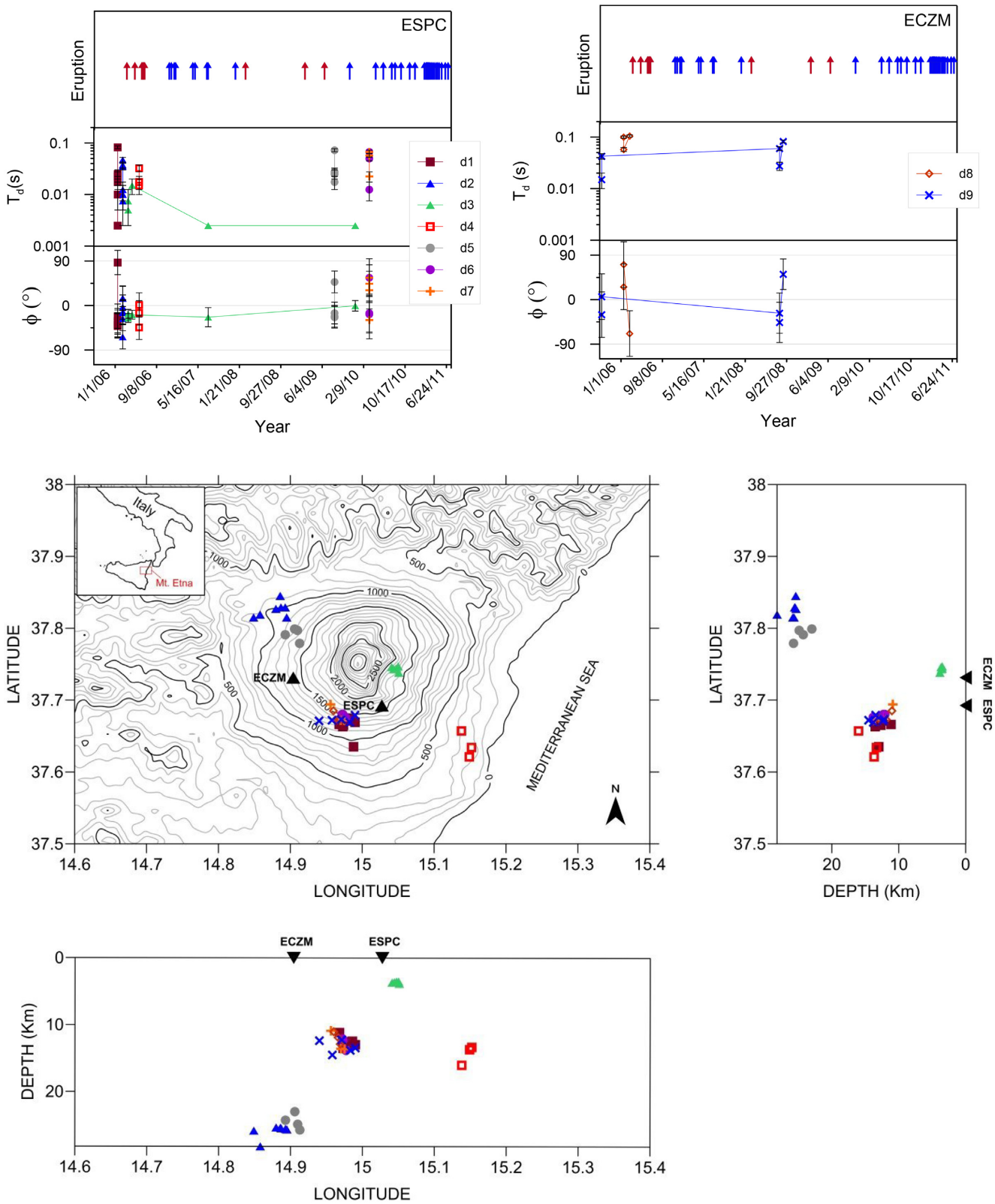

Figure 8. Top panel: selected multiplets for the station ESPC and ECZM versus the eruptions occurrence time (electrical blue arrows: summit eruptions; Red arrows: lateral eruptions). Each family of multiplets is marked by a different symbol. Bottom panel: epicentral and hypocentre locations of the selected multiplets in the two projections: east–west and north–south. Black triangles show the position of the two seismic stations.

Downloaded from https://academic.oup.com/gji/article-abstract/220/1/450/5585887 by INGV user on 03 December 2019

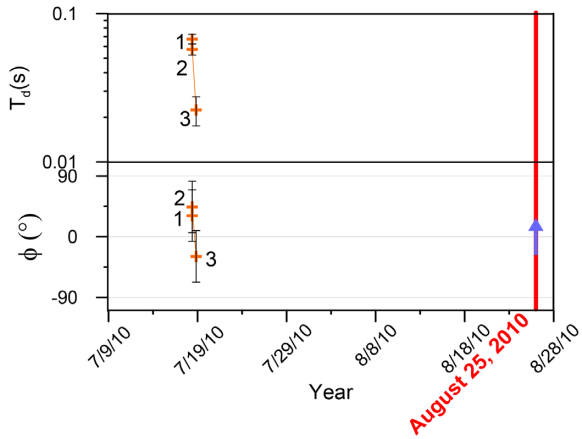

Figure 9. Selected multiplets of the family d7 for the station ESPC. The Electrical Blue arrow and the red line identify the eruption occurrence time. The number adjacent the orange cross identifies the single earthquake composing the multiplet family.

The analysis of multiplets highlights that before the eruption of 15 July 2006 (eruptive vents opened on the east and south flanks of the summit crater) ESPC, placed in the eastern unstable flank of the volcano, showed a variation in T_d and a 90°-flip in ϕ about 20 d before the eruption (d1 multiplet family). The same behaviour occurred about 30 d before the eruption of 25 August 2010 (explosion at the Bocca Nuova summit crater), d7 multiplet family (Figs 9 and S3 in the Additional_Supporting_Information of the Supplementary data). The changes at the ESPC station observed before the summit eruptions are probably caused by temporal spatially localized variations that do not allow to extrapolate a regularity in this behaviour within the observed database.

The 90°-flip, that we observed about 30 as well 20 d before the eruptions, may be the effects of the increasing pressure due to the magma rising towards the surface.

The multiplet family d3 (green triangle symbols in Fig. 8), that covered a very long period of time in the range 2006–2010 period, was the only one that showed no significant variations in polarization directions, and it was also the only multiplet family of shallow earthquakes (hypocentre depth around 3.5 km) located in the unstable flank of the volcano, into the Valle del Bove area.

ECZM station, placed instead in the west stable flank of the volcano, showed significant variations in T_d and 90°-flip of φ during the period 2008/2009 lateral eruption (northeast flank of the Northeast Crater). These variations are probably due to the decreasing stress acting on the area and the consequential increase in the total amount of fluid-filled microcracks. Furthermore, the 90°-flip can be the effect of both the relaxation of the stress and the eruption in the NE flank of Etna. Our results are consistent with those obtained by Bianco *et al*. (2006) related to the 2001 Etna's lateral and summit eruptions in the South flank of the volcano. Similarly, Zaccarelli *et al*. (2009) combining the SWS analysis with the Coda Wave Interferometry using the earthquake recorded at three stations placed on the NE sector of the volcano, have suggested that the temporal variation in T_d can be explained through the opening of new φ oriented microcracks produced by changes in either the relaxation of the stress field and the fluid content.

5 CONCLUSIONS

In this paper, we used Shear Wave Splitting analysis on a large number (1576) of earthquakes to investigate the spatial and temporal variation of anisotropy at Mt Etna. The analysis allowed us to identify three different sectors of the volcano defined by different representative polarization directions (Fig. 5). The NE sector is characterized by EW oriented polarization, while the SE sector has a quasi NS oriented polarization. Generally, the polarization direction is parallel to the maximum horizontal compressional stress and to the strike of vertical microcracks (Crampin & Peacock 2008 and references therein). In the SE unstable flank of the volcano the prevalent polarization directions identified by the SWS analysis, are consistent with the kinematic identified by Azzaro *et al*. (2013), because they are parallel to the fault strike and to the maximum horizontal compressive local volcanic stress direction responsible of the instability.

In the western sector of the volcano the polarization has two prevalent directions which are maybe controlled by the regional tectonic stress, given that reflect the about N–S striking compressive regime due to the convergence between the African and Eurasian plate and the extensional regime due to the dynamics of the Malta Escarpnet in the WNW–ESE direction.

Our data have not shown a clear link between the variations of the anisotropic parameters at all stations and the possible stress changes related to the eruptions. This is in agreement with the Etna open conduit system that experience volcanic eruptions almost continuously. The temporal variations observed in our results are related to single station measurements meaning the SWS parameter changes are related to very local stress field variations possibly linked to the impending eruption close by. Before both summit and lateral eruptions stations ECZM and ESPC exhibit significant variation in T_d, interpreted as due to a modification of the aligned fractures, and a 90°-flip of φ, which may be explained by over pressured fluids. This behaviour occurs when there is a change in the stress field, and it is probably related to the action of volcanic sources (inflation/deflation cycles) that influence the pore pressure. During the inflation the pore fluid pressure increases and reaches critical levels, the new stress field realigns modifying the distribution of microcracks and the fast shear wave does a 90°-flip, becoming parallel to the direction of the minimum horizontal stress. During the deflation, instead, the pore-fluid pressure is low and the polarization of the fast shear wave is parallel to the direction of the maximum horizontal stress, that for the SE part of the unstable flank correspond to a quasi NS oriented polarization.

Even though our results are consistent with those obtained by Bianco *et al*. (2006) and Zaccarelli *et al*. (2009), that showed precursory decreases immediately before the flank eruptions, we are not able to distinguishing the different kind of temporal variation in the anisotropic features as a function of the nature of the impending eruption (for instance summit eruption or flank eruption). More observations are needed to define the characteristic behaviour of the shear-wave splitting parameters for different types of eruption.

The outcome of this study is to provide a reference frame for spatial and temporal seismic anisotropy on Mt Etna with respect to the future temporal changes could be measured since in volcanic areas is important to distinguish between structural and stress induced anisotropy before interpreting shear wave splitting parameters and any time variations as caused by the dynamics of the volcanic activity.

Downloaded from https://academic.oup.com/gji/article-abstract/220/1/450/5585887 by INGV user on 03 December 2019

ACKNOWLEDGEMENTS

This research was partially supported by MED-SUV Project, funded by the European Union, and by OPTOFER Project—PON03PE-00155-1, funded by the MIUR. The authors wish to thank two anonymous reviewers for their helpful comments and suggestions, which significantly improved the manuscript.

REFERENCES

Acocella, V., Neri, M., Behncke, B., Bonforte, A., Del Negro, C. & Ganci, G., 2016. Why does a mature volcano need new vents? The case of the New Southeast Crater at Etna. *Front. Earth Sci.,* **4**.

Alparone, S., Barberi, G., Bonforte, A., Maiolino, V. & Ursino, A., 2011. Evidence of multiple strain fields beneath the eastern flank of Mt Etna volcano (Sicily, Italy) deduced from seismic and geodetic data during 2003–2004. *Bull. Volcanol.,* **73**(7), 869–885.

Alparone, S. *et al.*, 2015. Instrumental seismic catalogue of Mt. Etna earthquakes (Sicily, Italy): ten years (2000–2010) of instrumental recordings. *Ann. Geophys.,* **58**(4), S0435, doi:10.4401/ag-6591.

Azzaro, R., 1999. Earthquake surface faulting at Mount Etna volcano (Sicily) and implications for active tectonics. *J. Geodyn.,* **28**(2–3), 193–213.

Azzaro, R., Bonforte, A., Branca, S. & Guglielmino, F., 2013. Geometry and kinematics of the fault systems controlling the unstable flank of Etna volcano (Sicily). *J. Volc. Geotherm. Res.,* **251,** 5–15.

Barberi, G., Cocina, O., Neri, G., Privitera, E. & Spampinato, S., 2000. Volcanological inferences from seismic-strain tensor computations at Mt. Etna Volcano, Sicily, *Bull. Volcanol.,* **62,** 318–330

Battaglia, M., Gottsmann, J., Carbone, D. & Fernández, J., 2008. 4D volcano gravimetry. *Geophysics,* **73**(6), WA3–WA18.

Behncke, B., Fornaciai, A., Neri, M., Favalli, M., Ganci, G. & Mazzarini, F., 2016. Lidar surveys reveal eruptive volumes and rates at Etna, 2007–2010. *Geophys. Res. Lett.,* **43** (9), 4270–4278.

Bianco, F. & Castellano, M., 1997. The anisotropic volume of Mt. Etna: possible relationship with the stress field. *Acta Volcanol.,* **9**(1/2), 31–35.

Bianco, F., Scarfi, L., Del Pezzo, E. & Patanè, D., 2006. Shear wave splitting changes associated with the 2001 volcanic eruption on Mt. Etna. *Geophys. J. Int.,* **167**(2), 959–967.

Bianco, F., Zaccarelli, L., Del Pezzo, E. & Patanè, D., 2014. Seismic Anisotropy at Mt. Etna: massive measurements strategy and background state, in *Miscellanea INGV, MED-SUV 1th Year Meeting,* pp. 79–80, eds Puglisi, G. Spampinato, L. Reitano, D. & Mangiagli, S.

Bonforte, A., Guglielmino, F., Coltelli, M., Ferretti, A. & &Puglisi, G., 2011. Structural assessment of Mount Etna volcano from Permanent Scatterers analysis. *Geochem. Geophys. Geosyst.,* **12,** Q02002.

Cannata, A., Di Grazia, G., Aliotta, M., Cassisi, C., Montalto, P. & Patanè, D., 2013. Monitoring seismo-volcanic and infrasonic signals at volcanoes: Mt. Etna case study. *Pure appl. Geophys.,* **170**(11), 1751–1771.

Crampin, S., 1993. A review of the effects of crack geometry on wave propagation through aligned cracks. *Can. J. Explor. Geophys.,* **29,** 3–17.

Crampin, S. & Gao, Y., 2005. Comment on "Systematic analysis of shear-wave splitting in the aftershock zone of the 1999 Chi-Chi, Taiwan, Earthquake: shallow crustal anisotropy and lack of precursory changes, by Yungfeng Liu, Ta-Liang Teng, and Yehuda Ben-Zion". *Bull. seism. Soc. Am.,* **95**(1), 354–360.

Crampin, S. & Gao, Y., 2012. Plate-wide deformation before the Sumatra–Andaman Earthquake. *J. Asian Earth Sci.,* **46,** 61–69.

Crampin, S. & Gao, Y., 2013. The new geophysics. *Terra Nova,* **25**(3), 173–180

Crampin, S. & Peacock, S., 2005. A review of shear-wave splitting in the compliant crack-critical anisotropic Earth. *Wave Motion,* **41,** 59–77.

Crampin, S. & Peacock, S., 2008. A review of the current understanding of seismic shear-wave splitting in the Earth's crust and common fallacies in interpretation. *Wave Motion,* **45,** 675–722.

Crampin, S. & Zatsepin, S., 1997. Modelling the compliance of crustal rock-ii. response to temporal changes before earthquakes. *Geophys. J. Int.,* **129,** 495–506.

De Barros, L., Lokmer, I., Bean, C.J., O'Brien, G.S., Saccorotti, G., Métaxian, J.P., Zuccarello, L. & Patanè, D., 2011. Source mechanism of long-period events recorded by a high-density seismic network during the 2008 eruption on Mount Etna. *J. geophys. Res.,* **116,** B01304.

De Gori, P., Chiarabba, C. & Patanè, D., 2005. Qp structure of Mount Etna: constraints for the physics of the plumbing system. *J. geophys. Res.,* **1110,** B05303, doi:10.1029/2003JB002875.

De Gori, P., Chiarabba, C., Giampiccolo, E., Martinez-Arèvalo, C. & Patanè, D., 2011. Body wave attenuation heralds incoming eruptions at Mt. Etna. *Geology,* **39,** 503–506.

De Guidi, G. *et al.*, 2015. Geological, seismological and geodetic evidence of active thrusting and folding south of Mt. Etna (eastern Sicily): revaluation of "seismic efficiency" of the Sicilian Basal Thrust. *J. Geodyn.,* **90,** 32–41.

Del Negro, G. & Napoli, R., 2004. Magnetic field monitoring at Mt. Etna during the last 20 years, in *Mt. Etna: Volcano Laboratory,* **Vol. 143,** eds Bonaccorso, A., Calvari, S., Coltelli, M., Del Negro, C. & .Falsaperla, S, AGU, doi:10.1029/143GM15.

Del Pezzo, E., 2008. Seismic wave scattering in volcanoes. *Adv. Geophys.,* **50,** 353–371.

Del Pezzo, E., Ibáñez, J., Morales, J., Akinci, A. & Maresca, R., 1995. Measurements of intrinsic and scattering seismic attenuation in the crust. *Bull. seism. Soc. Am.,* **85**(5), 1373–1380.

Del Pezzo, E., Simini, M. & Ibáñez, J.M., 1996. Separation of intrinsic and scattering Q for volcanic areas: a comparison between Etna and Campi Flegrei. *J. Volc. Geotherm. Res.,* **70**(3), 213–219.

Del Pezzo, E., Bianco, F., Giampiccolo, E., Tusa, G. & Tuve, T., 2015. A reappraisal of seismic Q evaluated at Mt. Etna Volcano. Receipt for the application to risk analysis. *J. Seismol.,* **19**(1), 105–119.

Díaz-Moreno, A. *et al.*, 2018. New Insights on Mt. Etna's crust and relationship with the regional tectonic framework from joint active and passive P-wave seismic tomography. *Surv. Geophys.,* **39,** 57–97.

Nascimento, Do, F., A., Bezerra, F.H.R. & Takeya, M.K., 2004. Ductile Precambrian fabric control of seismic anisotropy in the Acu Dam area, northeastern Brazil. *J. geophys. Res.,* **109**(B10311), doi:10.1029/2004JB003120.002004.

Gambino, S., Mostaccio, A., Patanè, D., Scarfì, L. & Ursino, A., 2004. High-precision locations of the microseismicity preceding the 2002–2003 Mt. Etna eruption. *Geophys. Res. Lett.,* **31**(18), L18604.

Gao, Y, Wu, J., Fukao, Y, Shi, Y & Zhu, Ailan., 2011. Shear wave splitting in the crust in North China: stress, faults and tectonic implications. *Geophys. J. Int.,* **187,** 642–654.

Gerst, A. & Savage, M.K., 2004. Seismic anisotropy beneath Ruapehu Volcano: a possible eruption forecasting tool. *Science,* **306,** 1543–1547.

Giampiccolo, E., D'Amico, S., Patanè, D. & Gresta, S., 2007. Attenuation and source parameters of shallow microearthquakes at Mt. Etna volcano, Italy. *Bull. seism. Soc. Am.,* **97**(1B), 184–197.

Gledhill, K.R., 1991. Evidence for shallow and pervasive seismic anisotropy in the Wellington region, New Zealand. *J. geophys. Res.,* **96**(21), 503–521, 516.

Gresta, S., Peruzza, L., Slejko, D. & Distefano, G., 1998. Inferences on the main volcano tectonic structures at Mt. Etna (Sicily) from a probabilistic seismological approach. *J. Seismol.,* **2,** 105–116.

Ibáñez, J.M. *et al.*, 2016. The TOMO-ETNA experiment: an imaging active campaign at Mt. Etna volcano. Context, main objectives, working-plans and involved research projects. *Ann. Geophys.,* **59**(4), S0426, doi:10.4401/ag-7079.

Johnson, J. H., Savage, M. K. & Townend, J., 2011. Distinguishing between stress-induced and structural anisotropy at Mount Ruapehu Volcano, New Zealand. *J. geophys. Res.,* **116,** B12303.

Liu, S., Crampin, S., Luckett, R. & Yang, J., 2014. Changes in shear wave splitting before the 2010 Eyjafjallajökull eruption in Iceland. *Geophys. J. Int.,* **199,** 102–112.

Monaco, C., Tapponnier, P., Tortorici, L. & Gillot, P.Y., 1997. Late Quaternary slip rates on the Acireale–Piedimonte normal faults and tectonic origin of Mt. Etna (Sicily). *Earth planet. Sci. Lett.,* **147,** 125–139.

Downloaded from https://academic.oup.com/gji/article-abstract/220/1/450/5585887 by INGV user on 03 December 2019

Neri, M., Guglielmino, F. & Rust, D., 2007. Flank instability on Mount Etna: radon, radar interferometry and geodetic data from the southern boundary of the unstable sector. *J. geophys. Res.,* **112,** B04410.

Neri, M., Rivalta, E., Maccaferri, F., Acocella, V. & Cirrincione, R., 2018. Etnean and Hyblean volcanism shifted away from the Malta Escarpment by crustal stresses. *Earth planet. Sci. Lett.,* **486,** 15–22.

Nicolosi, I., D'Ajello Caracciolo, F., Branca, S., Ventura, G. & Chiappini, M., 2014. Volcanic conduit migration over a basement landslide at Mount Etna (Italy). *Sci. Rep.,* **4,** 5293.

O'Brien, G.S., Lokmer, I., De Barros, L., Bean, C.J., Saccorotti, G., Metaxian, J.P. & Patanè, D., 2011. Time reverse location of seismic long-period events recorded on Mt. Etna. *Geophys. J. Int.,* **184**(1), 452–462.

Patanè, D. & Privitera, E., 2001. Seismicity related to 1989 and 1991–93 Mt. Etna (Italy) eruptions: kinematic constraints by fault plane solution analysis. *J. Volc. Geotherm. Res.,* **109**(1–3), 77–98, ISSN 0377-0273.

Patanè, D., De Gori, P., Chiarabba, C. & Bonaccorso, A., 2003. Magma ascent and the pressurization of Mt. Etna's volcanic system. *Science,* **299,** 2061–2063.

Patanè, D., Cocina, O., Falsaperla, S., Privitera, E. & Spampinato, S., 2004. Mt. Etna volcano: a seismological framework, in *The Mt. Etna Volcano,* pp. 147–165, Calvari, S., Bonaccorso, A., Coltelli, M., Del Negro, C. & Falsaperla, S., eds, AGU.

Patanè, D., Mattia, M. & Aloisi, M., 2005. Shallow intrusive processes during 2002–2004 and current volcanic activity at Mt. Etna. *Geophys. Res. Lett.,* **32,** L06302.

Patanè, D., Barberi, G., Cocina, O., De Gori, P. & Chiarabba, C., 2006. Time-resolved seismic tomography detects magma intrusions at Mount Etna. *Science,* **313,** 821.

Patanè, D. *et al.*, 2013. Insights into magma and fluid transfer at Mount Etna by a multiparametric approach: a model of the events leading to the 2011 eruptive cycle. *J. geophys. Res.,* **118,** 1–21.

Rasmussen, D.J., Plank, T.A., Roman, D.C., Power, J.A., Bodnar, R.J. & Hauri, E.H., 2018. When does eruption run-up begin? Multidisciplinary insight from the 1999 eruption of Shishaldin volcano. *Earth planet. Sci. Lett.,* **486,** 1–14, ISSN 0012–821X.

Rust, D., Behncke, B., Neri, M. & Ciocanel, A., 2005. Nested zones of instability in the Mount Etna volcanic edifice, Sicily. *J. Volc. Geotherm. Res.,* **155,** 137–153.

Savage, M. K., Ohminato, T., Aoki, Y., Tsuji, H. & Greve, S. M., 2010. Stress magnitude and its temporal variation at Mt. Asama Volcano, Japan, from seismic anisotropy and GPS. *Earth planet. Sci. Lett.,* **290**(3), 403–414.

Scarfì, L., Barber, G., Musumeci, C. & Patanè, D., 2016. Seismotectonics of northeastern Sicily and southern Calabria (Italy): new constraints on the tectonic structures featuring in a crucial sector for the central Mediterranean geodynamics. *Tectonics,* **35,** 812–832.

Torelli, L., Grasso, M., Mazzoldi, G. & Peis, D., 1998. Plio-Quaternary tectonic evolution and structure of the Catania foredeep, the northern Hyblean Plateau and the Ionian shelf (SE Sicily). *Tectonophysics,* **298,** 209–221.

Viccaro, M., Zuccarello, F., Cannata, A., Palano, M. & Gresta, S., 2016. How a complex basaltic volcanic system works: Constraints from integrating seismic, geodetic, and petrological data at Mount Etna volcano during the July–August 2014 eruption. *J. geophys. Res.,* **121,** 5659–5678.

Zaccarelli, L. & Bianco, F., 2008. A shear wave analysis system for semi-automatic measurements of shearwave splitting above volcanic earthquakes: descriptions and applications, in *Conception, Verification and Application of Innovative Techniques to Study Active Volcanoes,* eds Marzocchi, W. & Zollo, A., INGV–DPC, Rome, pp. 113–124, ISBN978-88-89972-09-0.

Zaccarelli, L., Pandolfi, D., Bianco, F., Saccorotti, G., Bean, C.J. & Del Pezzo, E., 2009. Temporal changes in seismic wave propagation towards the end of the 2002 Mt Etna eruption. *Geophys. J. Int.,* **178,** 1779–1788.

Zaccarelli, L., Bianco, F. & Zaccarelli, R., 2012. Splitting parameter yield (SPY): a program for semiautomatic analysis of shear-wave splitting. *Comput. Geosci.,* **40,** 138–145.

Zatsepin, S. & Crampin, S., 1997. Modelling the compliance of crustal rock: I - response of shear-wave splitting to differential stress. *Geophys. J. Int.,* **129,** 477–494.

Zhang, Z. & Schwartz, S.Y., 1994. Seismic anisotropy in the shallow crust of the Loma Prieta segment of the San Andreas fault system. *J. geophys. Res.,* **99,** 9651–9661.

Zinke, J.C. & Zoback, M.D., 2000. Structure-related and stress-induced shear-wave velocity anisotropy: observations from microearthquakes near the Calaveras Fault in central California. *Bull. seism. Soc. Am.,* **90,** 1305–1312.

SUPPORTING INFORMATION

Supplementary data are available at *GJI* online.

Figure S1. Hypocentral distribution of the 2006–2011 earthquakes. The grey points represent the shallow earthquakes and the black points represent the deep earthquakes.

Figure S2. time delay T_d (s) versus hypocentral distance. Correlation coefficients (CC) between T_d and distance are marked on top of each panel.

Figure S3. representation of the anisotropic parametrization of the earthquakes of the family d7. On the left the horizontal component (EW and NS) seismograms with *P* and *S* arrivals as vertical red lines. On the right four sub plots are: (a) the superimposed horizontal components (EW in blue and NS in black) of the seismograms with the fast and slow split shear-wave arrivals as straight and dotted red lines, respectively; (b) the particle motion (N versus E amplitude) of the event inside the covariance window, starting at t_S; (c) the horizontal seismograms zoomed around the covariance window (which is highlighted by the vertical lines) and (d) the three curves represented are the fast component (continuous blue line), the slow components (continuous black line), and the slow one corrected by the time delay found (black dotted line).

Please note: Oxford University Press is not responsible for the content or functionality of any supporting materials supplied by the authors. Any queries (other than missing material) should be directed to the corresponding author for the paper.

Downloaded from https://academic.oup.com/gji/article-abstract/220/1/450/5585887 by INGV user on 03 December 2019